10.1098/rspa.2002.1044

THE ROYAL SOCIETY

Effect of thermo- and diffusiophoretic forces on the motion of flame-generated particles in the neighbourhood of burning droplets in microgravity conditions

By G. Ben-Dor, T. Elperin and B. Krasovitov

Department of Mechanical Engineering, The Pearlstone Center for Aeronautical Engineering Studies, Ben-Gurion University of the Negev, PO Box 653, Beer-Sheva 84105, Israel (elperin@menix.bgu.ac.il)

Received 25 February 2002; revised 19 June 2002; accepted 24 June 2002; published online 20 January 2003

Numerical analysis of the effect of thermo- and diffusiophoretic forces on the motion of moderately large ($0.01 \lesssim Kn \lesssim 0.3$) combustion-generated (soot) particles and on the formation of soot-shell structure in the buoyancy-free spherical droplet flames is performed. Transient evaporation, ignition and combustion of a single sooting-fuel droplet immersed into a quiescent hot environment are considered, taking into account the effects of radiative heat losses, variable transport properties and the dependence of the droplet surface temperature on time. Results of numerical calculations are compared with available experimental data and recent theoretical models. We calculated thermo- and diffusiophoretic and total velocities of combustion-generated particles and showed that soot particles form a size-segregated soot-shell structure. Within a soot shell the particles with smaller radii are located closer to the droplet surface, while larger particles are located closer to the flame front. Numerical calculations performed for moderately large soot particles showed that there are two equilibrium locations, where the total velocity is equal to zero, between the droplet and the flame front. It is found that one of the equilibrium locations is the point of unstable equilibrium and the other position is the point of stable equilibrium. We numerically determined the dependence of soot-shell-to-droplet-diameter ratios on the particle radius.

Keywords: droplet combustion; microgravity; thermophoresis; diffusiophoresis; soot particles

1. Introduction

Numerous analytical models and numerical simulations of droplet combustion and microgravity burner-generated spherical-diffusion flames have been performed in the past. Discussions of these studies can be found in the review papers by Law (1982) and Ronney (1998). Kadota *et al*. (1977) and Kadota & Hiroyasu (1984) investigated soot formation during droplet combustion and observed that soot is formed in a thin layer between the droplet surface and the flame front. As was shown in experiments at normal gravity (Randolph & Law 1986), even the weak convective flows can reduce

soot emission and soot agglomeration significantly. Thus, Randolph & Law (1986) used low pressure to reduce, and thereby to control, buoyancy. They studied various dynamic factors that can strongly influence the extent of soot formation in droplet burning. It was shown (Randolph & Law 1986) that, as long as the flame encloses the soot, it will eventually be oxidized as the flame regresses inwards. Thus, near-complete combustion, with or without microexplosion, should result in very little soot emission. However, early extinction of the flame removes the oxidation barrier and will lead to a significant amount of soot emission.

Soot formation during microgravity combustion of hydrocarbon fuels was observed in recent experimental studies on combustion of a single droplet of different hydrocarbon fuels (Shaw *et al.* 1988; Hara & Kumagai 1990; Jackson *et al.* 1991, 1994; Jackson *et al.* 1992; Avedisian *et al.* 1998).

The reduced-gravity experiments on sooting-fuel-droplet combustion were performed by Shaw *et al.* (1988) to exhibit an initial period of approximately d-square-law combustion, followed by a sudden flame contraction and then growth, and sometimes disruption (where d is the particle diameter).

Hara & Kumagai (1990) conducted experiments for free n-heptane droplet combustion under microgravity. They found that at the early stage of burning, the soot shell formed is almost spherical, and then the soot starts to form a tail at some location on the shell. At the final stage of burning, the soot disappeared and only the soot tail was observed.

An experimental study concerning the influence of liquid composition on soot formation and burning rate of a droplet composed of highly sooting fuel (toluene) and non-sooting fuel (methanol) was performed by Jackson *et al.* (1991). The experimental observations were made in a microgravity environment to achieve near spherically symmetric burning of the droplets. This study demonstrated the effect of composition on soot formation in the burning of isolated and stationary alcohol–aromatic mixture droplets. Jackson *et al.* (1992) observed the soot dynamics and the formation of soot-shell structure in droplet-combustion experiments performed in a low-gravity environment.

During fuel-droplet combustion, the temperature and concentration distributions in the neighbourhood of a droplet are strongly inhomogeneous. In this case the thermo- and diffusiophoretic forces caused by temperature and concentration gradients affect the soot particles located in the neighbourhood of the burning droplets. In spherically symmetric droplet flames the effects of thermo- and diffusiophoresis lead to soot accumulation between the droplet and flame front. Transport of soot inside and outside of the flame is dominated by the drag force in the Stefan flow and by thermophoretic and diffusiophoretic forces arising due to high temperature and concentration gradients. Therefore, in order to describe the soot shell in a spherically symmetric diffusion-flame environment correctly, the motion of the flame-generated particles in the neighbourhood of the burning droplets must be accounted for.

As has been noted before (Randolph & Law 1986; Jackson *et al.* 1992; Avedisian *et al.* 1998) the location of the soot-shell structure is expected to be determined by the inwardly directed thermophoretic forces which balance the outwardly directed drag forces acting on soot agglomerates. Earlier thermo- and diffusiophoretic effects were incorporated into the theoretical model of in-cloud scavenging of large, moderately large and small aerosol particles by Yalamov *et al.* (1977), who showed that thermo-

and diffusiophoresis dominate Brownian diffusion for large and moderately large aerosol particles.

The duration of low-gravity experiments in drop towers is determined by the distance of the fall. Drop towers provide experimental times from 100 ms to 10 s (for towers as high as 1670 ft (*ca.* 510 m)). Longer time requirements can be satisfied by using aircraft undergoing parabolic flight trajectories, sounding rockets or the Space Shuttle (Avedisian 1997).

The fibre-supported droplet-combustion experiment on spherically symmetric droplet combustion was conducted in the Spacelab aboard the Space Shuttle during the STS-73 mission (Williams *et al.* 1996). The experimental apparatus allowed the study of combustion of large methanol and heptane–hexadecane droplets in air. The initial diameters of the droplets were 2–5 mm. The tests performed for sooting-fuel droplets (heptane–hexadecane mixture) showed that a droplet *ca.* 5 mm in diameter issued enormous amounts of soot, far more than expected. This study showed that the initial diameter seemingly has a large effect on the amount of soot produced.

Nayagam *et al.* (1999) presented results of experiments on the combustion of freely floated *n*-heptane droplets in 300 K helium–oxygen environments conducted in the Spacelab onboard the Space Shuttle Columbia during the first launch (STS-83) of the Microgravity Science Laboratory mission in April 1997. These results demonstrated both radiative and diffusive flame extinction during burning, whereas droplet-surface regression followed a *d*-square-law. Nayagam *et al.* (1999) also determined soot standoff ratios as a function of time.

Previous theoretical studies concerning the effect of the soot shell on transient droplet combustion and microgravity burner-generated spherical-diffusion flames considered mainly two aspects of the problem: modelling of soot formation, oxidation and agglomeration and the effect of a soot shell on radiative heat losses. In particular, Chang & Shien (1995) investigated single-droplet combustion theoretically, taking into account the flame-radiation effect. In the latter study, the experimental data on soot-layer thickness and soot volume fraction were used. Ezekoye & Zhang (1997) investigated soot oxidation and agglomeration in microgravity-maintained spherical diffusion flames theoretically. Soot and gas radiation was calculated by Ezekoye & Zhang (1997), using the spherical harmonics P_1 approximation. Soot evolution was studied using various combinations of the existing soot-radiation models. Baek *et al.* (1999), using the non-grey radiation model for the radiative heat-transfer equation, investigated single-droplet combustion including soot formation and flame radiation. The discrete ordinate method was employed to solve the radiation-transfer equation, and the weighted-sum-of-grey-gases model was applied to account for the non-grey-gas-radiation effect by CO_2 and H_2O, while soot was assumed to be grey (Baek *et al.* 1999).

In this study we presented results of the theoretical analysis of the transient evaporation, ignition and combustion of a single sooting-fuel droplet immersed into a quiescent radiative environment. The model takes into account the effects of gas–soot-mixture radiation. We also investigated the dynamics of flame-generated particles. Analysis of the stability points of soot-shell structure is performed based on three different velocity terms (Stefan-flow velocity, thermo- and diffusiophoretic velocities).

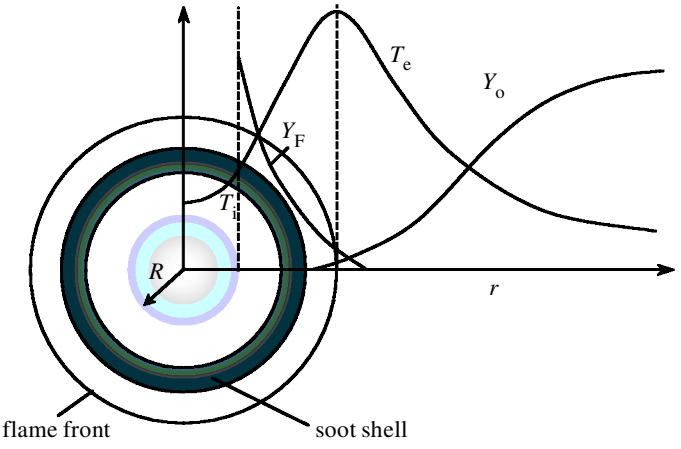

Figure 1. Schematic of a burning sooting-fuel droplet.

2. Mathematical model

(a) *Combustion of monocomponent fuel droplet*

Consider a spherical droplet of a pure fuel with radius R_0 immersed into a stagnant, hot, gaseous mixture with temperature T_∞. It is assumed that the effect of buoyancy is small. This assumption can be achieved under microgravity conditions. The droplet is heated by a conduction heat flux from the high-temperature surroundings and evaporates. Ignition can be attained in the case when the energy delivered to any volume of the combustible mixture is larger then the minimum spontaneous ignition energy. Since the chemical reaction rate is a nonlinear function of gaseous species concentrations and temperature, after a certain time-interval (corresponding to the ignition delay) a rapid temperature rise in the neighbourhood of the droplet occurs and an enveloping flame appears around the droplet. The soot shell then forms between the droplet and flame front, as shown in figure 1.

In further analysis, the following simplifying assumptions are made: spherical symmetry; effects of buoyancy are small; Dufour–Soret and viscous dissipation effects are neglected.

Under these restrictions, the mass, species and energy-conservation equations describing the spherically symmetric gaseous phase surrounding the droplet read

$$r^2\frac{\partial \rho}{\partial t}+\frac{\partial}{\partial r}(r^2\rho v_r)=0, \tag{2.1}$$

$$r^2\frac{\partial}{\partial t}(\rho Y_i)+\frac{\partial}{\partial r}(\rho v_r r^2 Y_i)=\frac{\partial}{\partial r}\left(\rho D_i r^2\frac{\partial Y_i}{\partial r}\right)+r^2(\nu_i''-\nu_i')M_i\dot{\omega}, \tag{2.2}$$

$$r^2\frac{\partial(\rho c_p T_e)}{\partial t}+\frac{\partial}{\partial r}(\rho v_r r^2 c_p T_e)=\frac{\partial}{\partial r}\left(k_e r^2\frac{\partial T_e}{\partial r}\right)+r^2 M_F Q\dot{\omega}-r^2\nabla \boldsymbol{Q}_R, \tag{2.3}$$

where t is the time, r is the radial coordinate, ρ is the density of gaseous mixture, v_r is the radial component of gas velocity, c_p is the specific heat at constant pressure, $i=\overline{1,K}$ is the number of gaseous phase species, Y_i and M_i are the mass fraction and the molar mass of the ith species (the subscript 'F' denotes the ith species

corresponding to fuel vapour), respectively, D_i is the diffusion coefficient, ν_i'' and ν_i' are the stoichiometric coefficients of the product and the reactant, k_e and T_e are the coefficient of thermal conductivity of gaseous mixture and the temperature of gaseous phase surrounding it, $\dot{\omega}$ is the rate of chemical reaction, Q is specific heat of chemical reaction and $\boldsymbol{Q}_\mathrm{R}$ is the radiation flux vector.

Estimations of the characteristic values of the terms $\partial\rho/\partial t$ and $\nabla(\rho\boldsymbol{v})$ in the continuity equation (2.1) show that $\partial\rho/\partial t \ll \nabla(\rho\boldsymbol{v})$ when $v^2/c^2 \ll 1$ (where v is the gas velocity and c is the sound velocity). The radial gas velocity (Stefan velocity) at the droplet surface can be evaluated (see, for example, Marchese & Dryer 1996) as

$$v_{r,\mathrm{S}} = \frac{\rho_\mathrm{l}}{\rho}\bigg|_{r=R} \frac{K_\mathrm{b}}{8R}, \tag{2.4}$$

where ρ_l is the liquid density and K_b is the burning rate constant. Simple calculations show that, for an n-heptane droplet 1 mm in initial diameter with $\rho_\mathrm{l} \approx 621\ \mathrm{kg\,m^{-3}}$ burning in air ($\rho \sim 1\ \mathrm{kg\,m^{-3}}$, $K_\mathrm{b} \sim 10^{-6}\ \mathrm{m^2\,s^{-1}}$ for typical hydrocarbon fuels at atmospheric pressure), the radial gas velocity at the droplet surface is of the order of $0.16\ \mathrm{m\,s^{-1}}$. Here, in evaluating Stefan velocity, a constant value of K_b was assumed. Notably, recent experiments on nonane–hexanol-mixture droplet combustion conducted by Avedisian & Callahan (2000) showed that dilution of nonane by hexanol decreases the droplet burning rate, which was found to be time dependent. As can be seen from these estimations, the Stefan velocity is much smaller than the sound velocity. Thus, for the solution of heat and mass-conservation equations (2.1)–(2.3), describing the spherically symmetric gaseous phase surrounding the burning droplet, instead of equation (2.1) we can use an anelastic approximation

$$\frac{\partial}{\partial r}(r^2\rho v_r) = 0. \tag{2.5}$$

The above system of partial differential equations must be supplemented by the momentum-conservation equation. However, in the case of subsonic flow velocities (low-Mach-number approximation) the pressure gradient arising is negligibly small ($\Delta p \sim \rho v^2 \sim 10^{-2}\ \mathrm{Pa}$) and, therefore, the pressure can be assumed to be constant. The gaseous-phase properties can be related through the ideal gas equation of state

$$p = p_\infty = \rho R_\mathrm{g} T \sum_{i=1}^{K} \left(\frac{Y_i}{M_i}\right), \tag{2.6}$$

where R_g is the universal gas constant and p_∞ is the gaseous-mixture pressure far from the droplet. The radial flow velocity

$$\rho v_r r^2 = \rho_\mathrm{S} v_{r,\mathrm{S}} R^2 = -\frac{\dot{m}_\mathrm{l}}{4\pi} \tag{2.7}$$

can be found from the continuity equation (2.5), where $\dot{m}_\mathrm{l}$ is the mass rate of droplet vaporization. Since the problem under consideration involves moving boundaries, we transform a spatial coordinate system to a fixed domain where the receding droplet interface is immobilized. Introducing the variables

$$x = \frac{r}{R(t)}, \qquad \tau = \frac{\alpha_\mathrm{l} t}{R_0^2}, \qquad \theta_\mathrm{e} = \frac{T_\mathrm{e}}{T_{\mathrm{e},\infty}},$$

$$\xi(\tau) = \frac{R(t)}{R_0}, \qquad \zeta_T = \frac{1}{\alpha_\mathrm{l}\rho c_p}, \qquad \zeta_D = \zeta_T c_p,$$

we obtain the system of dimensionless energy- and mass-conservation equations

$$\Psi[Y_i, \zeta_D, \rho D_i, M_i(\nu_i'' - \nu_i'), 0] = 0, \tag{2.8}$$

$$\Psi[\theta_{\mathrm{e}}, \zeta_T, k_{\mathrm{e}}, QM_{\mathrm{F}}T_\infty^{-1}, 1] = 0. \tag{2.9}$$

The operator $\Psi[\phi, \beta, \gamma, \lambda, \chi]$ in equations (2.8) and (2.9) is defined as

$$\Psi[\phi,\beta,\gamma,\lambda,\chi] = \xi^2\frac{\partial\phi}{\partial\tau} - x\xi\dot{\xi}\frac{\partial\phi}{\partial x} + u\frac{\xi R_0}{\alpha_{\mathrm{l}}}\frac{\partial\phi}{\partial x} - \frac{\beta}{x^2}\frac{\partial}{\partial x}\left(x^2\gamma\frac{\partial\phi}{\partial x}\right) + \beta\xi R_0\left(\frac{\chi}{x^2T_\infty}\frac{\partial}{\partial x}(x^2\boldsymbol{Q}_{\mathrm{R}}\cdot\boldsymbol{n}) - \lambda\xi R_0\dot{\omega}\right), \tag{2.10}$$

where $u = u(x,\tau)$ is the gas velocity and the thermophysical properties ρ, D_i, k_{e} and c_p are functions of the new independent variables x and τ, $\boldsymbol{n}$ is the unit normal vector, $\dot{\omega}$ is the mass-production rate of the ith species by the gas-phase one-step chemical reaction given by the Arrhenius formula (Westbrook & Dryer 1981)

$$\dot{\omega} = Z\left(\frac{\rho Y_{\mathrm{F}}}{M_{\mathrm{F}}}\right)^a\left(\frac{\rho Y_{\mathrm{o}}}{M_{\mathrm{o}}}\right)^b\exp\left(-\frac{E_{\mathrm{a}}}{R_{\mathrm{g}}\theta_{\mathrm{e}}T_\infty}\right), \tag{2.11}$$

where E_{a} is the activation energy and Z is the pre-exponential constant. The gaseous phase velocity u and the rate of change of the droplet radius $\dot{\xi}$ can be determined as follows (Ben-Dor *et al.* 2003):

$$u(x,\tau) = -\frac{1}{x^2}\frac{\rho_{\mathrm{l}}\alpha_{\mathrm{l}}}{\rho R_0}\dot{\xi}(\tau), \tag{2.12}$$

$$\dot{\xi}(\tau) = \frac{1}{\xi(\tau)}\frac{\rho_{\mathrm{S}}D_{\mathrm{F,S}}(\partial Y_{\mathrm{F}}/\partial x)|_{x=1}}{\rho_{\mathrm{l}}\alpha_{\mathrm{l}}(1-Y_{\mathrm{F,S}})}. \tag{2.13}$$

In equations (2.12) and (2.13), α_{l} is the liquid thermal diffusivity and subscript 'S' denotes the value at the droplet surface.

Initial and boundary conditions read

$$\theta_{\mathrm{e}}(0,x) = \theta_{\mathrm{e}}^{(0)}(x), \qquad Y_i(0,x) = Y_i^{(0)}(x), \tag{2.14}$$

$$\frac{1}{u}\frac{D_{\mathrm{F}}}{\xi R_0}\frac{\partial Y_{\mathrm{F}}}{\partial x}\bigg|_{x=1} = (1-Y_{\mathrm{F}})|_{x=1}, \tag{2.15}$$

$$\frac{1}{u}\frac{D_i}{\xi R_0}\frac{\partial Y_i}{\partial x}\bigg|_{x=1} = Y_i|_{x=1} \quad (i = \overline{2,K}), \tag{2.16}$$

$$\frac{k_{\mathrm{e}}}{k_{\mathrm{l}}}\frac{1}{\xi}\left(\frac{\partial\theta_{\mathrm{e}}}{\partial x}\right)\bigg|_{x=1} = -\frac{L}{c_{\mathrm{l}}T_\infty}\frac{\mathrm{d}\xi(\tau)}{\mathrm{d}\tau}\bigg|_{x=1} + \frac{\xi}{3}\frac{\mathrm{d}\theta_{\mathrm{e}}}{\mathrm{d}\tau}\bigg|_{x=1} + \frac{R_0}{k_{\mathrm{l}}T_\infty}(\boldsymbol{Q}_{\mathrm{R}}\cdot\boldsymbol{n})\bigg|_{x=1}, \tag{2.17}$$

$$Y_{\mathrm{F,S}}(\theta_{\mathrm{S}}) = \exp\left(-\frac{LM_{\mathrm{F}}}{R_{\mathrm{g}}T_{\mathrm{b}}}\left(\frac{T_{\mathrm{b}}}{\theta_{\mathrm{S}}T_\infty} - 1\right)\right). \tag{2.18}$$

In equation (2.17), k_{l} is the coefficient of thermal conductivity of a liquid and c_{l} is the specific heat of a liquid. The second term on the right-hand side of equation (2.17)

is the fraction of the dimensionless heat flux required for droplet heating and the third term on the right-hand side of (2.17) is the radiative flux.

At $x \to \infty$ and $\tau > 0$, the soft boundary conditions at infinity,

$$\left.\frac{\partial \theta_{\mathrm{e}}}{\partial x}\right|_{x\to\infty} = \left.\frac{\partial Y_i}{\partial x}\right|_{x\to\infty} = 0 \quad (i = \overline{1, K}), \tag{2.19}$$

are imposed.

(*b*) *Radiative heat transfer*

In order to model the effect of non-luminous radiative heat losses from the droplet flame, we used the approach by Saitoh *et al.* (1993). The radiative flux divergence $\nabla \boldsymbol{Q}_{\mathrm{R}}$ can be obtained by integrating the radiative-transfer equation written in terms of the spherical coordinate system under the assumption of isotropic scattering,

$$\frac{1}{x^2}\frac{\partial}{\partial x}(x^2 \boldsymbol{Q}_{\mathrm{R}} \cdot \boldsymbol{n}) = \kappa_{\mathrm{P}} \xi R_0 (4E_{\mathrm{b}} - G(x)), \tag{2.20}$$

where E_{b} is the black-body emitted flux and the irradiance $G(x)$ is given by

$$G(x) = \int_{\Omega=4\pi} I(x,\eta)\,\mathrm{d}\Omega = 2\pi \int_{-1}^{1} I(x,\eta)\,\mathrm{d}\eta, \quad \eta = \cos\vartheta, \tag{2.21}$$

where I is the radiation intensity. For a mixture of combustion products (CO_2 and water vapour) and soot particles in non-absorbing carrier gas, the Planck mean absorption coefficient κ_{P} in equation (2.20) can be written as

$$\kappa_{\mathrm{P}} = \kappa_{\mathrm{P,g}}(\theta_{\mathrm{e}}) + \kappa_{\mathrm{P,s}}(\theta_{\mathrm{e}}), \tag{2.22}$$

where $\kappa_{\mathrm{P,g}}(T_{\mathrm{e}})$ and $\kappa_{\mathrm{P,s}}(T_{\mathrm{e}})$ are the Planck mean absorption coefficients for gaseous combustion products and soot, respectively. The Planck mean absorption coefficient $\kappa_{\mathrm{P,g}}$ for the gaseous combustion products CO_2 and H_2O can be calculated by

$$\kappa_{\mathrm{P,g}}(\theta_{\mathrm{e}}) = P(y_{\mathrm{CO_2}} \kappa_{\mathrm{P,CO_2}}(\theta_{\mathrm{e}}) + y_{\mathrm{H_2O}} \kappa_{\mathrm{P,H_2O}}(\theta_{\mathrm{e}})), \tag{2.23}$$

where P is the pressure (in atm) and y is the molar fraction of the species. The following expression was used to calculate $\kappa_{\mathrm{P},j}$ for H_2O and CO_2 (Roekaerts *et al.* 2000):

$$\kappa_{\mathrm{P},j} = \sum_m A_{j,m} \theta_{\mathrm{e}}^m. \tag{2.24}$$

Total emissivity of the soot shell ϵ_{s} is given by (Felske & Tien 1973)

$$\epsilon_{\mathrm{s}} = 1 - \frac{15}{\pi^4}\psi^{(3)}\left[1 + \frac{c_0 f_{\mathrm{v}} T_{\mathrm{e}} l}{C_2}\right], \tag{2.25}$$

where $\psi^{(3)}$ is the pentagamma function

$$\psi^{(n)}(z) = \frac{\mathrm{d}^{n+1}}{\mathrm{d}z^{n+1}} \ln \Gamma(z) = (-1)^{n+1} \int_0^\infty \frac{t^{n+1} \mathrm{e}^{-zt}}{1 - \mathrm{e}^{-t}}\,\mathrm{d}t, \quad \mathrm{Re}(z) > 0, \quad n = 1, 2, 3, \ldots,$$

c_0 is a constant which was set equal to 5.0, $C_2 = ch/k_{\mathrm{B}} = 14\,388\ \mu\mathrm{m\ K}$ (where c is the speed of light) is the second Planck constant, f_{v} is the volume fraction of soot,

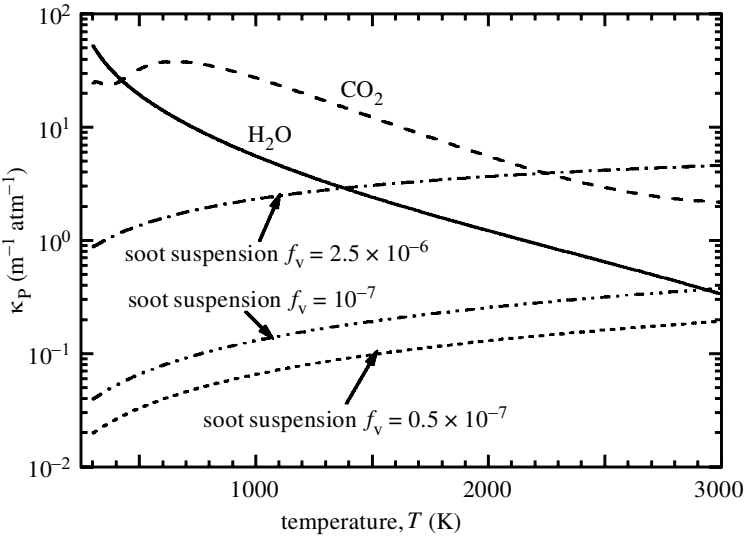

Figure 2. Planck mean absorption coefficient of soot suspension for CO_2 and H_2O.

T_e is the ambient temperature of the soot-gas mixture and l is the thickness of the soot shell. Different values of soot volume fraction f_v are reported in the literature. f_v varies between 7.0×10^{-8} and 1.0×10^{-7}, as was determined by Abdel-Khalik *et al.* (1974). Lee *et al.* (1984) found that the values of f_v are in the range 10^{-7}–10^{-5} and, according to Siegel & Howell (1981), the values vary from 10^{-8} to 10^{-6}. Resent measurements (Choi *et al.* 1995) performed in the post-flame region of an acetylene–air premixed flame showed that the value of soot fraction is of the order of 10^{-5}.

The Planck mean absorption coefficient $\kappa_{P,s}$ can be calculated using Beer's law:

$$\kappa_{P,s} = -\frac{1}{l}\ln(1-\epsilon_s). \tag{2.26}$$

Results of the numerical calculations of the coefficients κ_{P,CO_2}, κ_{P,H_2O} and $\kappa_{P,s}$ are shown in figure 2. As can be seen from this plot for soot volume fractions of the order of 10^{-8} and lower, the effect of the radiation absorption by the soot shell is small in comparison with radiation absorption by the gaseous combustion products (CO_2 and water vapour).

(*c*) *Thermo- and diffusiophoretic motion of flame-generated soot particles*

The location of the combustion-generated particle (see figure 3) between the droplet and the flame front is determined by the balance between the inwardly directed thermophoretic forces and the outwardly directed drag forces and diffusiophoretic forces which act on soot particles formed during the combustion of sooting-fuel droplets. Outside the flame front, outwardly directed thermo- and diffusiophoretic and drag forces propel soot particles away from the flame front. The production of soot particles in a flame is a chemically controlled process. The initial size of the soot particles is of the order of 10–30 nm. However, when soot particles are formed, they grow quickly by surface growth and collisional coagulation. In the

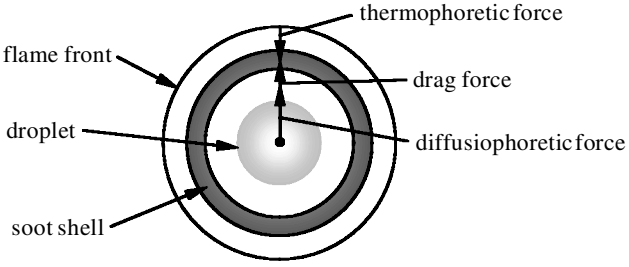

Figure 3. Schematic of a droplet, a soot shell and a flame.

present study we consider the dynamics of moderately large ($0.01 \lesssim Kn \lesssim 0.3$) flame-generated agglomerates with fairly complex morphologies. It is assumed that these agglomerates can be modelled as solid spheres with the effective radius $R_{\rm p}$ and the effective thermal conductivity k_p. This assumption can be questionable. However, the structure of flame-generated aggregates shows some evidence of fractal-like properties. The latter can simplify their morphological description as it was demonstrated experimentally and supported by several theoretical studies (Köylü *et al.* 1995*a*; Brasil *et al.* 2001). Recent experimental investigations (Manzello & Choi 2002) showed that at the earlier stage of droplet-combustion soot particles form cluster–cluster fractal-like aggregates with a fractal dimension $D_{\rm f}$ in the range from 1.59 to 1.61. Aggregates may then undergo the restructuring process, whereby their open-branched structure collapses, resulting in a more compact cluster, i.e. particle–cluster fractal-like aggregates with large fractal dimension ($D_{\rm f} = 2.75$) (Brasil *et al.* 2001). Strictly speaking, such particle–cluster fractal-like aggregates must be considered as porous spheres. However, in compact clusters, in the case of point contact of the particles, the diameter of the pores may not exceed the diameter of the particle (i.e. 10–30 nm). In this case the aggregate can be modelled as a solid sphere at the surface of which the diffusion reflection of the gas molecules occurs (i.e. the accommodation coefficient is equal to unity). Recently, direct measurements of the thermophoretic force acting on polystyrene latex (PSL) spheres and aggregates were conducted by Zheng & Davis (2001), who determined equivalent volume radii, thermophoretic and dynamic shape factors for different types of aggregates of PSL spheres (doublets, triangular and V-shaped triplets and Y-shaped quadruplets). They showed that the thermophoretic-force data for non-spherical particles corrected by the measured shape factors are in fairly good agreement with theoretical models by Waldman (1959), Talbot *et al.* (1980), Loyalka (1992) and Yamamoto & Ishihara (1988).

The velocity of a soot particle located in the field of temperature and concentration gradients can be expressed as the sum of three terms,

$$\boldsymbol{v}_r = \boldsymbol{u} + \boldsymbol{v}_{\rm tp} + \boldsymbol{v}_{r,{\rm dp}}, \tag{2.27}$$

where the gas, thermophoretic and diffusiophoretic velocities ($\boldsymbol{u}$, $\boldsymbol{v}_{\rm tp}$ and $\boldsymbol{v}_{\rm dp}$, respectively) are the functions of x and τ. Well-established theory of the thermophoresis (Brock 1962; Bakanov *et al.* 1979) of large aerosol particles assumes that the thermophoretic velocity can be obtained from the solution of the linearized system of steady-state Navier–Stokes and energy conservation equations with slip boundary conditions at the surface of the particle. In the case of moderately large aerosol particles, the boundary conditions must include kinetic terms that are the functions of

temperature jump, Knudsen number, etc. Thus, the above model can be used as long as

(i) the Stokes time $\tau_{\rm s}$ is much less then the characteristic time-scale for droplet combustion $\tau_{\rm drop}$, i.e.

$$\tau_{\rm s} = \frac{2}{9}\frac{R_{\rm p}^2}{\mu}\rho_p \ll \tau_{\rm drop} = \frac{d_0^2}{K_{\rm b}};$$

(ii) the nonlinear terms in momentum and energy conservation equations are much less then the linear terms.

Since thermophoretic velocity is of the order of

$$v_{\rm tp} \sim \frac{\mu}{\rho T_{\rm e}}|\nabla T_{\rm e}|,$$

it is easily seen that the condition for the validity of the model is $(R_{\rm p}|\nabla T_{\rm e}|)/T_{\rm e} \ll 1$.

Simple estimations show that, for a soot particle with a radius of 1 μm and density $\rho = 1.8\ {\rm g\ cm^{-3}}$ moving in the vicinity of the burning n-heptane droplet 0.4 mm in diameter, the Stokes time is of the order of 10^{-4} s, whereas the characteristic time-scale for droplet combustion is ~ 0.2 s. Since $(R_{\rm p}|\nabla T_{\rm e}|)/T_{\rm e} \sim 10^{-3} \ll 1$, the above approach can be applied to model thermo- and diffusiophoretic motion of flame-generated particles in the vicinity of the burning droplet.

The current theory of thermophoresis of solid particles in a gas at low Knudsen numbers (Kn) yields the thermophoretic velocity (Bakanov 1992, 1995)

$$\boldsymbol{v}_{\rm tp} = -f_{\rm T}\frac{\mu}{\rho}\frac{\nabla T_{\rm e}}{T_{\rm e}}, \tag{2.28}$$

where

$$f_{\rm T} = K_{\rm tsl}\frac{1 + Kn\cdot\Phi}{1 + k_p/(2k_{\rm e})} \tag{2.29}$$

and Φ is a function of the momentum accommodation coefficient α^*, energy accommodation coefficient ε and the ratio of thermal conductivity coefficients $k_p/k_{\rm e}$. In the most general form, the function $\Phi(\varepsilon, \alpha^*, k_p/k_{\rm e})$ reads

$$\Phi\left(\varepsilon, \alpha^*, \frac{k_p}{k_{\rm e}}\right) = A(\varepsilon, \alpha^*)\frac{k_p}{k_{\rm e}} + D(\varepsilon, \alpha^*) + \frac{B(\varepsilon, \alpha^*) + C(\varepsilon, \alpha^*)(k_p/k_{\rm e})}{1 + (k_p/(2k_{\rm e}))}. \tag{2.30}$$

Compilation of the values of the coefficients A, B, C and D obtained in various studies can be found in Bakanov (1992, 1995). In the present study we adopt the coefficients $A = 2.26$, $B = 0.55$, $C = -2.18$, $D = -0.15$ and $\varepsilon = \alpha^* = 1$ obtained by Poddoskin *et al.* (1982). The gas-kinetic approach was applied by Poddoskin *et al.* (1982) to derive the velocity distribution function in the case of arbitrary momentum and energy accommodation. This result was applied to determine kinetic boundary conditions at the particle's surface. The boundary conditions were then used by Poddoskin *et al.* (1982) to calculate the thermophoretic velocity of a moderately large aerosol particle.

As can be seen from expressions (2.29) and (2.30), the thermophoretic velocity depends on the ratio $k_p/k_{\rm e}$, where k_p is the effective thermal conductivity of the

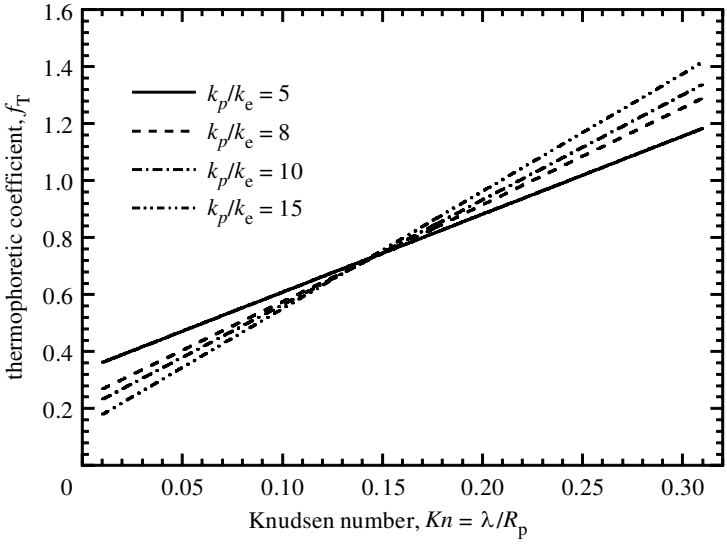

Figure 4. Thermophoretic coefficient f_T against Knudsen number $Kn = \lambda/R_p$ at various thermal conductivity ratios.

spherical soot aggregate. In the case when aggregate (porous sphere) consists of spherical particles with random arrangement the relation k_p/k_e can be estimated by Krupitczka's correlation (Krupitczka 1967)

$$\frac{k_p}{k_e} = \left(\frac{k_{sp}}{k_e}\right)^{0.280 - 0.757 \log \varepsilon - 0.057 \log(k_{sp}/k_e)}, \tag{2.31}$$

where k_{sp} is thermal conductivity of the solid phase (carbon), k_e is thermal conductivity of the external gaseous mixture, and ε is the porosity of the agglomerate (in the case of spherical particles with random arrangement, ε varies from 0.38 to 0.46).

Due to high-temperature differences thermal conductivity of the gaseous mixture in the neighbourhood of a burning droplet varies significantly. However, simple estimations with Krupitczka's correlation (2.31) showed that the ratio k_p/k_e is of the order of 10 with a small variation (approximately from 8.2 to 12.9). As is shown in figure 4, in this range the thermophoretic coefficient f_T (2.29) has only a weak dependence on k_p/k_e for Knudsen numbers in the range $0.01 \lesssim Kn \lesssim 0.3$. Thus, we can consider the ratio k_p/k_e to be constant and calculate at the reference temperature that for inner and outer region can be calculated using Sparrow's one-third rule (Hubbard *et al.* 1975):

$$T_r^{(i)} = \tfrac{1}{3}T_S + \tfrac{2}{3}T_f, \tag{2.32}$$

$$T_r^{(o)} = \tfrac{1}{3}T_f + \tfrac{2}{3}T_\infty. \tag{2.33}$$

In equations (2.32) and (2.33) $T_r^{(i)}$ and $T_r^{(o)}$ are the reference temperature at the inner and outer regions, respectively, T_S is the temperature at the droplet surface, T_f is the flame front temperature and T_∞ is the temperature at infinity.

The expression for the diffusiophoretic velocity of aerosol particle in multicomponent gaseous mixture was derived by Viehland & Mason (1977). In a frame attached

to the droplet this expression reads

$$\boldsymbol{v}_{\mathrm{dp}} = \sum_{i=1}^{K-1} \frac{nD_i^*}{\rho}\left(\nabla y_i + \sum_{j=1}^{K} y_i y_j \alpha_{ij} \nabla \ln T_{\mathrm{e}}\right), \tag{2.34}$$

where y_i and y_j are molar fractions of the ith and jth species respectively, $\alpha_{ij} = -\alpha_{ji}$ is the multicomponent thermal diffusion factor, n is the total number density and the ρ is the total mass density of the gas. The coefficient D_i^* can be calculated as the ratio of two determinants (Viehland & Mason 1977)

$$D_i^* = \frac{\det \hat{D}_i}{\det \tilde{D}}, \tag{2.35}$$

where the denominator is determined by

$$\det \tilde{D} = \begin{vmatrix} \dfrac{1}{D_{1\mathrm{s}}} & \dfrac{1}{D_{2\mathrm{s}}} & \dfrac{1}{D_{3\mathrm{s}}} & \cdots & \dfrac{1}{D_{K-1\mathrm{s}}} & \dfrac{1}{D_{K\mathrm{s}}} \\ -\displaystyle\sum_{j=2}^{K} \dfrac{y_j}{\mathcal{D}_{1j}} & \dfrac{y_1}{\mathcal{D}_{12}} & \dfrac{y_1}{\mathcal{D}_{13}} & \cdots & \dfrac{y_1}{\mathcal{D}_{1K-1}} & \dfrac{y_1}{\mathcal{D}_{1K}} \\ \dfrac{y_2}{\mathcal{D}_{12}} & -\displaystyle\sum_{\substack{j=1 \\ j\neq 2}}^{K} \dfrac{y_j}{\mathcal{D}_{2j}} & \dfrac{y_2}{\mathcal{D}_{23}} & \cdots & \dfrac{y_2}{\mathcal{D}_{2K-1}} & \dfrac{y_2}{\mathcal{D}_{2K}} \\ \vdots & \vdots & \vdots & \ddots & \vdots & \vdots \\ \dfrac{y_{K-2}}{\mathcal{D}_{1K-2}} & \dfrac{y_{K-2}}{\mathcal{D}_{2K-2}} & \dfrac{y_{K-2}}{\mathcal{D}_{3K-2}} & \cdots & \dfrac{y_{K-2}}{\mathcal{D}_{K-2K-1}} & \dfrac{y_{K-2}}{\mathcal{D}_{K-2K}} \\ \dfrac{y_{K-1}}{\mathcal{D}_{1K-1}} & \dfrac{y_{K-1}}{\mathcal{D}_{2K-1}} & \dfrac{y_{K-1}}{\mathcal{D}_{3K-1}} & \cdots & \displaystyle\sum_{\substack{j=1 \\ j\neq K-1}}^{K} \dfrac{y_j}{\mathcal{D}_{K-1j}} & \dfrac{y_{K-1}}{\mathcal{D}_{K-1K}} \end{vmatrix}. \tag{2.36}$$

In expression (2.36), $\mathcal{D}_{ij} = \mathcal{D}_{ji}$ are mutual diffusion coefficients. The numerator for $\det \hat{D}_i$ is obtained from expression (2.36) by replacing the $(i+1)$th row by $\{m_1, m_2, \ldots, m_{K-1}, m_K\}$. The expressions for Brownian gas particle diffusion coefficients $D_{1\mathrm{s}}$ (Viehland & Mason 1977) are given by

$$D_{1\mathrm{s}} = \frac{a_i \Lambda_i}{6\pi R_{\mathrm{p}} \mu n (1 - \Delta_{i\mathrm{s}})}, \tag{2.37}$$

where $\Lambda_i = (\mu/R_{\mathrm{p}})(\pi k_{\mathrm{B}} T/(2m_i))^{1/2}$, k_{B} is the Boltzmann constant, m_i is the mass of the ith species molecule,

$$1 - \Delta_{i\mathrm{s}} \approx \frac{1 + c_i(\Lambda_i/p)}{1 + b_i(\Lambda_i/p)}$$

and a_i, b_i and c_i are the dimensionless parameters of order 1.

3. Numerical method

The system of nonlinear parabolic partial differential equations (2.8), (2.9) was integrated numerically using the method of lines (Sincovec & Madsen 1975). This method was employed to reduce the system of nonlinear partial parabolic differential equations (2.8), (2.9) to a system of ordinary differential equations. The system of equations was approximated by a system of ordinary differential equations in time for the values of T and Y_i at the mesh points. The resulting system of ordinary differential equations was solved using the backward-differentiation formula. In the case of droplet combustion, the temperature and concentration gradients inside the domain between the droplet and the flame front are very steep. Therefore, the mesh points outside the droplet were spaced adaptively using the formula

$$x_i = x_1 + (x_N - x_1)\left[1 - \cos\left(\frac{\pi}{2}\frac{(i-1)}{(N-1)}\right)\right], \tag{3.1}$$

so that they clustered near the left-hand boundary, where gradients are steep. In equation (3.1) N is the chosen number of mesh points and x_1 and x_N are the locations of the left- and right-hand boundaries, respectively. Generally, in the numerical solution, 651 mesh points and an error tolerance of *ca.* 10^{-4} in time integration are employed. In order to verify the convergence of the adopted numerical procedure, calculations were performed with grids having 651, 801 and 1001 mesh points. Since the results showed that sufficient accuracy is attained using a grid with 651 mesh points, all the calculations in this study were performed with a grid having this number of mesh points. Variable time-steps were used to improve the computational accuracy and efficiency.

One of the main factors that affect stable computation is the selection of the initial profiles of temperature and mass fraction. Thus, for a droplet evaporating and igniting in a hot radiant atmosphere, the following formulae for these profiles were assumed. For $i \geqslant 1$,

$$\theta_i = \theta_N + (\theta_1 - \theta_N)[1 - \tfrac{1}{2}\pi \arctan(\omega[x_i - 1])], \tag{3.2}$$

$$Y_i = Y_N + (Y_1 - Y_N)[1 - \tfrac{1}{2}\pi \arctan(\omega[x_i - 1])], \tag{3.3}$$

where ω is the parameter that determines the steepness of the initial profile. During numerical solution of equations (2.8) and (2.9) the properties ρ, c_p, D_i and k_e are evaluated simultaneously at each grid point for each iteration. The dependence of ρ, c_p, D_i and k_e on temperature and concentration of gaseous mixture species is taken into account. Using the calculated temperature and concentration profiles, the thermo- and diffusiophoretic velocities and total velocity of flame-generated moderately large particles were calculated. The mean free path of the molecules λ is recalculated at each time-step. For the mean free path λ of the molecules we used the viscosity-based value. Properties of the liquid as well as of the gaseous phase are adopted from Reid *et al.* (1987), Vargaftik (1975) and Chase (1998).

4. Results and discussion

The model described above for combustion of a sooting-fuel droplet in a hot and radiant environment was applied to study the process of soot accumulation between

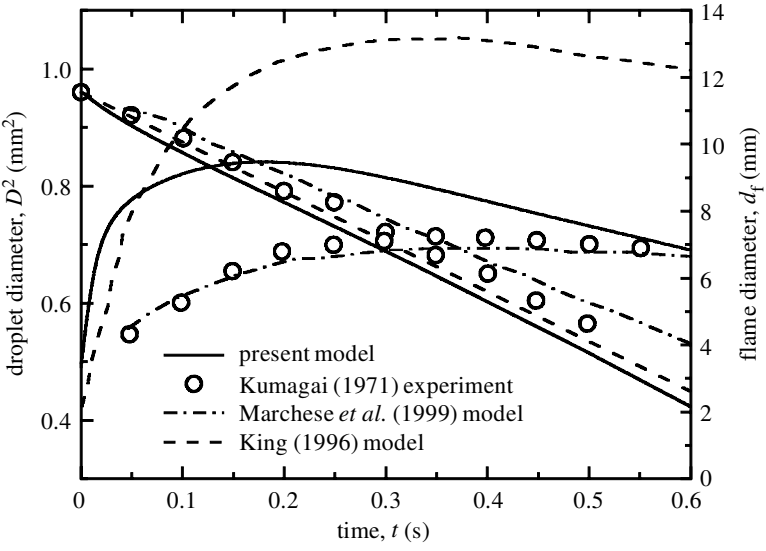

Figure 5. Comparison of the calculated results with experimental results of Kumagai *et al.* (1971) and numerical results of King (1996) and Marchese *et al.* (1999). Initial conditions: initial droplet diameter, 0.98 mm; temperature at infinity, 298 K; air at 1 atm pressure.

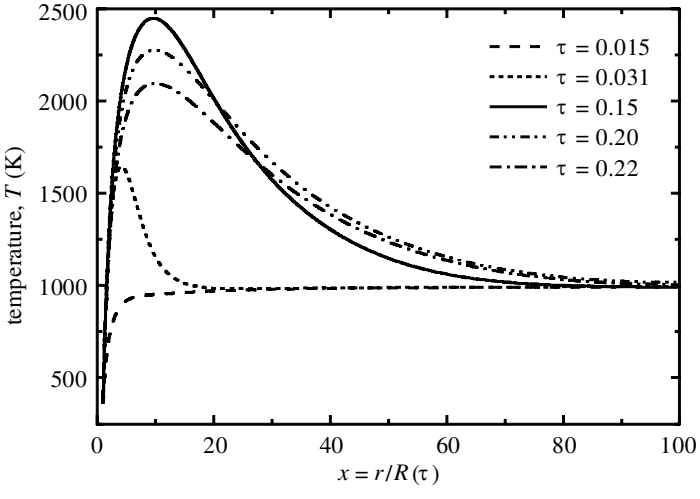

Figure 6. Variations of the calculated temperature versus dimensionless distance $x = r/R(\tau)$ at various instances of time for n-heptane droplet ($R_0 = 200$ μm, $T_\infty = 1000$ K).

the droplet and the flame front during transient combustion of a single fuel droplet, taking into account the effects of radiation and variable transport properties. Using this model, we also analysed the dynamics of combustion-generated soot particles. The calculations were performed for n-heptane droplet evaporating, igniting and burning in hot air.

A comparison of the present model of droplet combustion with the experimental data of Kumagai *et al.* (1971) and the recent numerical results of King (1996) and Marchese *et al.* (1999) for a 0.98 mm diameter n-heptane droplet burning in air at

atmospheric pressure is given in figure 5. The numerical model suggested by King (1996) considered a transient-droplet combustion with an infinite rate of chemical reaction, temperature-dependent thermophysical properties and unit Lewis number. Droplet heating and radiative heat losses were not taken into account. Marchese *et al.* (1999) simulated combustion of a single multicomponent n-alkane droplet numerically with a model that includes gas-phase detailed multicomponent molecular transport and complex chemical kinetics. As can be seen from figure 5, the predicted results are consistent with the reported experimental data and numerical results. Inspection of figure 5 shows that the results obtained are in good agreement with experimental data (Kumagai *et al.* 1971) and numerical models (King 1996; Marchese *et al.* 1999) for droplet diameter as a function of time. For the flame diameter as a function of time, the numerical results of this study are in better agreement with the experimental data than with the numerical calculation of King (1996) but in worse agreement than the prediction of Marchese *et al.*'s (1999) model. Note in this connection the importance of combustion models including complex chemical kinetics. These models allow us to calculate concentrations of the reaction products (such as CO_2, H_2O, CO, etc.) that may have an appreciable effect on the thermal conductivity, radiative heat loss and flame-temperature decrease. The latter affects the flame diameter. Note that the one-step chemical reaction model does not include the production of CO, which affects the radiative heat loss.

Calculations were performed for an isolated n-heptane droplet with initial radius $R_0 = 200$ μm evaporating, igniting and burning in a hot air with temperature $T_\infty = 1000$ K and normal atmospheric pressure. Figure 6 shows transient-gas-temperature profiles for various instants of time. The initial temperature of the droplet is assumed to be 280 K. As can be seen from this plot, the gas temperature increases rapidly after ignition due to combustion and reaches *ca.* 2500 K. Then the temperature maximum decreases as a result of radiative heat losses.

As mentioned above, transport of flame-generated particles inside and outside the flame is determined by the drag force and thermo- and diffusiophoretic forces arising due to high temperature and concentration gradients. Soot particles are formed due to chemically controlled processes during combustion of hydrocarbon fuels and they can grow through the surface chemical reactions and collisional coagulation. The chemically controlled surface growth of soot particles is fairly fast. Thus, in the region between the droplet and the flame front, the soot particles are propelled inward as long as thermophoretic force is larger than diffusiophoretic and drag forces. The balance between the inwardly directed thermophoretic forces and outwardly directed drag and diffusiophoretic forces determines the location of the soot-shell structure. For an n-heptane droplet burning in air, in the zone between the droplet and the flame front concentration of oxidizer is low. On the other hand, radicals such as OH can oxidize the soot particles. In any case, chemical reaction cannot change appreciably the imposed external temperature gradient at the soot particle due to droplet combustion. Thus, the effect of chemical reaction at the surface of particles was neglected. The thermo- and diffusiophoretic velocities of moderately large ($0.01 \lesssim Kn \lesssim 0.3$) flame-generated particles of different radii were calculated using the calculated temperature and concentration profiles. Measurements based on thermophoretic sampling showed that flame-generated soots range from small aggregates (with sizes of the order of 10 nm) near the start of soot formation to large aggregates (with sizes of the order of 1 μm) (Köylü *et al.* 1995*b*). Calcula-

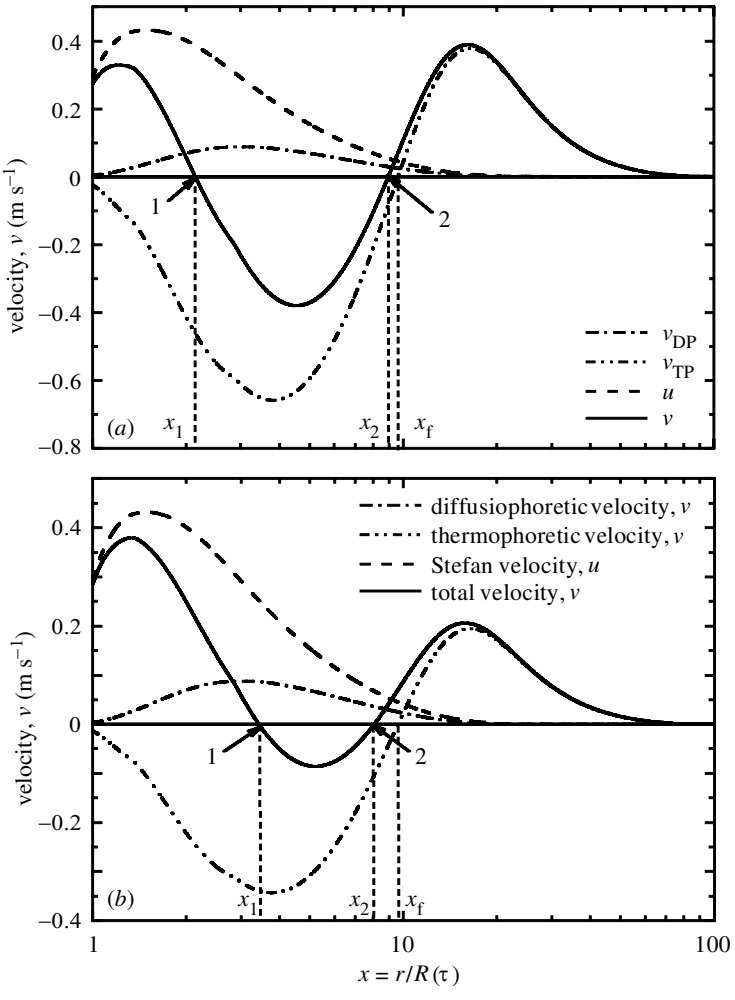

Figure 7. Calculated diffusiophoretic, thermophoretic, Stefan and total velocities of soot particle versus dimensionless distance $x = r/R(\tau)$. (*a*) $\tau = 0.15$, $R_p = 0.5$ μm; (*b*) $\tau = 0.15$, $R_p = 1.0$ μm.

tions were performed for soot particles with radii 0.5 μm (figure 7*a*) and 1.0 μm (figure 7*b*) located in the field of temperature and concentration gradients formed near the burning *n*-heptane droplet at time $\tau = 0.15$. According to equation (2.25), the total velocity of the particle is the sum of the gas, thermophoretic and diffusiophoretic velocities. Figure 7 shows the instantaneous values of gas velocity and thermophoretic, diffusiophoretic and total velocities of the flame-generated particles with radii 0.5 μm and 1 μm against the non-dimensional radial distance $x = r/R(\tau)$. In these plots the negative value of the velocity implies inwardly directed particle motion. As can be seen from figure 7, thermophoretic and drag forces are dominant in comparison with the diffusiophoretic force. However, these results show that the effect of the diffusiophoretic force is significant and must be taken into account. Numerical results presented in figure 7 show that the particles located between the droplet surface and location 2 with the dimensionless radial coordinate $x = x_2$ are accumulated between the droplet surface and the flame front (x_f is the dimensionless

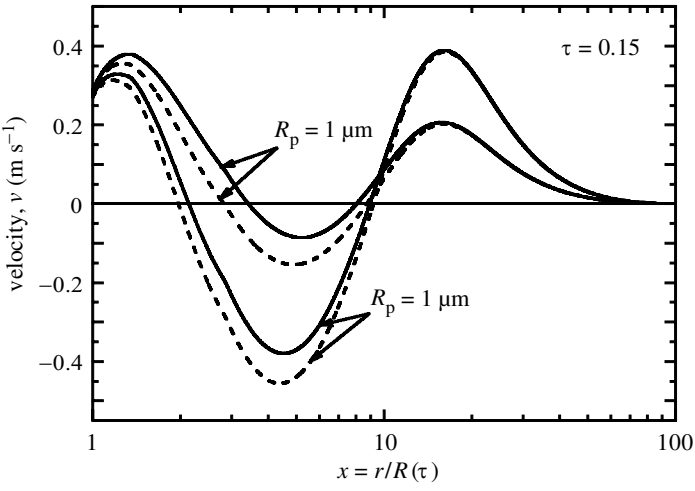

Figure 8. Total velocities of soot particles with radii 0.5 μm and 1 μm; solid lines, diffusiophoresis is taken into account; dashed lines, diffusiophoresis is neglected.

radial coordinate of the flame front location), while particles located further from the droplet surface are withdrawn into the flame front due to the dominant drag force. Outside the flame front, soot particles move away from the flame front due to the outwardly directed thermophoretic, diffusiophoretic and drag forces. Numerical calculations performed for moderately large particles show that there are two equilibrium locations (points 1 and 2 in figure 7) between the droplet and the flame front where the total velocity is equal to zero. However, it is easily seen that one of the equilibrium locations (point 2) is the point of unstable equilibrium, whereas another position (point 1) is the point of the stable equilibrium. Note that the existence of two equilibrium (stable and unstable) locations was first discussed by Jackson & Avedisian (1996). Their inference was based on the analysis of the dimensionless net force variation in the neighbourhood of a burning *n*-heptane droplet. Our arguments on the analysis of the stable and unstable positions are basically the same. However, diffusiophoretic force was not included in the calculations performed by Jackson & Avedisian (1996). Figure 8 shows the instantaneous values of the total velocities of the flame-generated particles with radii 0.5 μm and 1 μm. In this plot the dashed lines denote the results obtained neglecting the diffusiophoretic force. As can be seen from figure 8, the effect of diffusiophoresis is significant, and neglecting the diffusiophoretic force can result in the error in total velocity and soot-shell location.

Variations of the instantaneous values of the total particle velocity are shown against the non-dimensional coordinate in figure 9. The curves are plotted for the particles with radii 0.2, 0.5 and 1.0 μm. Analysis of these numerical results shows that, within a soot shell, the particles with lesser radii are located closer to the droplet surface, while larger particles are located closer to the flame front. Thus, it can be concluded that combustion-generated particles form the size-segregated soot-shell structure.

Figure 10 presents the time evolution of the calculated total velocity of the particle with radius 0.5 μm against non-dimensional distance $x = r/R(\tau)$. These results show that, for soot particles with radii of *ca.* 0.5 μm, the soot-shell stand-off ratio d_s/d is

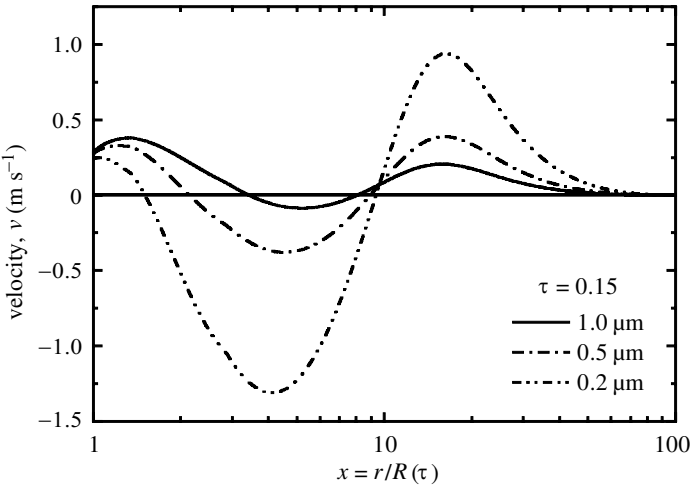

Figure 9. Variation of the calculated total velocities of soot particles of different radii plotted against dimensionless distance $x = r/R(\tau)$.

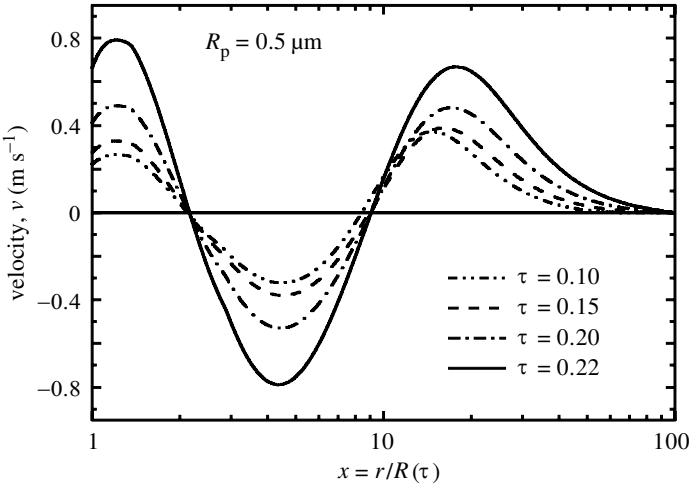

Figure 10. Variations of the calculated total velocities of soot particle ($R_\mathrm{p} = 0.5$ μm) against dimensionless distance $x = r/R(\tau)$ at various instances of time.

fairly constant. Such a constant soot-shell-to-droplet-diameter ratio was observed experimentally by Jackson & Avedisian (1994). We performed numerical calculations of the dependence of soot-shell-to-droplet-diameter ratios (d_s/d) on the mean radius of a soot particle (figure 11). As can be seen from this plot the soot-shell-to-droplet-diameter ratios do not depend practically on time for the particles with radii less than 0.6 μm. The experimental measurements of variation of soot-shell-to-droplet-diameter ratios with time reported by Jackson & Avedisian (1994) (see figure 12) showed that, for *n*-heptane droplets, soot-shell-to-droplet-diameter ratios vary in the range from 2 to 3.5. As can be seen from figure 12, numerical results obtained in this study are consistent with the experimental observations for the soot particles with radii in the range 0.45–0.8 μm. The small increase in soot-shell-to-

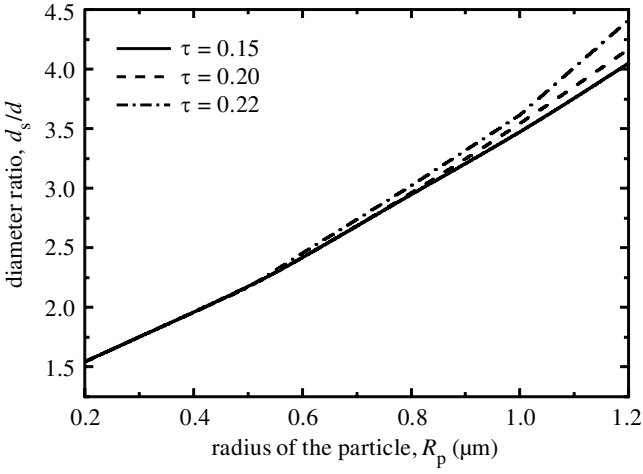

Figure 11. Variations of the soot-shell-to-droplet-diameter ratios plotted against soot particle radius at various instances of time.

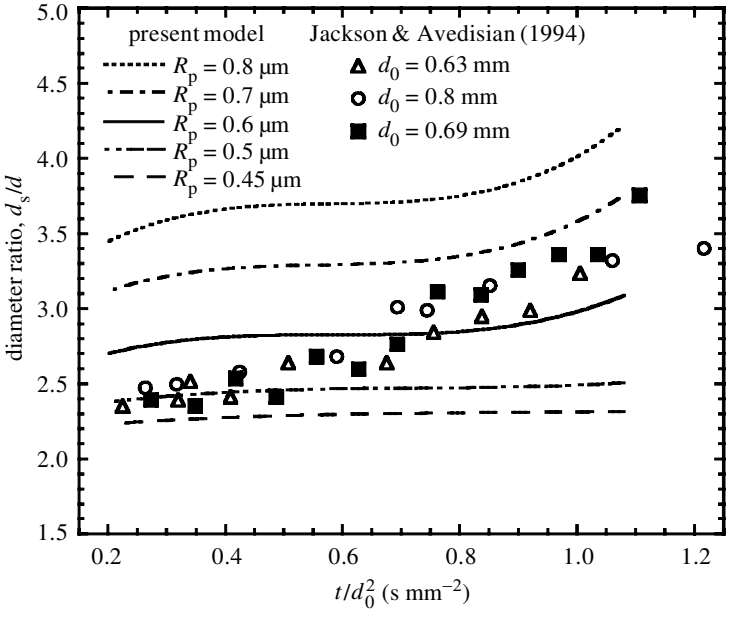

Figure 12. Variation of soot-shell-to-droplet-diameter ratio against time for various R_p.

droplet-diameter ratios during droplet combustion observed by Jackson & Avedisian (1994) can be associated with the coagulation growth of soot particles. Comparing the dependencies of soot-shell-to-droplet-diameter ratio versus time calculated using the present model with the experimental data obtained by Jackson & Avedisian (1994) for a 0.63 mm diameter *n*-heptane droplet allowed us to determine the time dependence of the mean soot aggregates' radii (see figure 13). Herewith, the experimental dataset was approximated by a linear function using the least-squares method. As can be seen from figure 13, during combustion of the *n*-heptane droplet

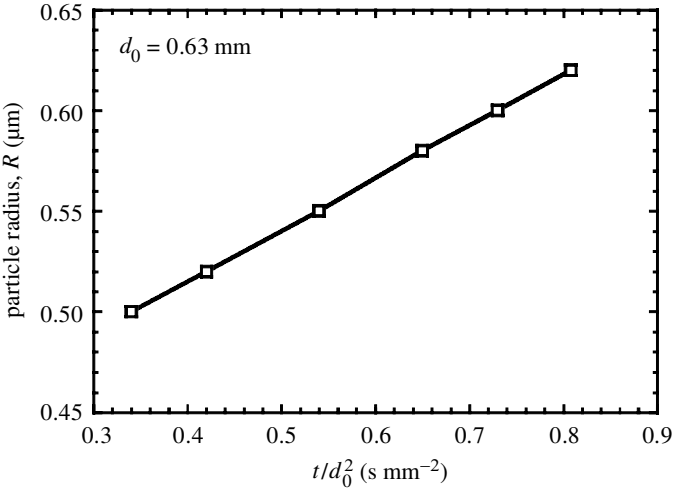

Figure 13. Variation of the mean size of soot aggregates against time during droplet combustion.

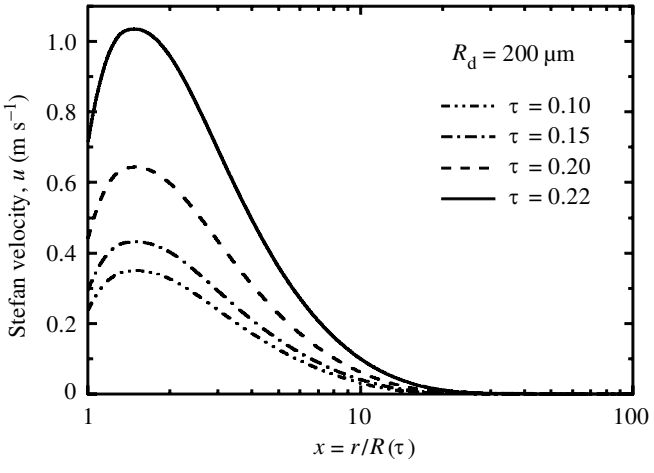

Figure 14. Variations of the Stefan velocity versus dimensionless distance $x = r/R(\tau)$ at various instances of time.

with initial diameter 0.63 mm, the mean radius of the soot aggregates grows linearly with time in the range 0.5–0.62 μm. Thus, experimental data on time variation of soot-shell-to-droplet-diameter ratios allow us to determine the mean soot-aggregate size growth with time during droplet burning using the inverse procedure and the developed model. The calculations performed showed that the location of the particles for which the soot-shell-to-droplet-diameter ratio d_s/d is constant in time is in the vicinity of the maximum of the Stefan velocity. As can be seen from figure 14, the maximum of Stefan velocity versus normalized coordinate $x = r/R(\tau)$ is constant in time. Thus, for the soot particles located in the vicinity of the maximum of Stefan velocity, the soot-shell-to-droplet-diameter ratio d_s/d will be constant in time.

5. Conclusions

Transport of flame-generated particles inside and outside the flame is determined by the drag force and thermophoretic and diffusiophoretic forces arising due to high temperature and concentration gradients. The location of a combustion-generated particle between the droplet and the flame front is determined by the balance between the inwardly directed thermophoretic forces and the outwardly directed drag forces and diffusiophoretic forces which act on soot particles formed during combustion of sooting-fuel droplets. Outside the flame front, soot particles move away from the flame front. We investigated numerically the effect of thermo- and diffusiophoretic forces on the motion of moderately large ($0.01 \lesssim Kn \lesssim 0.3$) flame-generated soot particles and on the formation of a soot-shell structure in the buoyancy-free spherical droplet flames. Transient evaporation, ignition and combustion of a single sooting-fuel droplet immersed into a stagnant hot environment is considered, taking into account the effects of radiative heat losses and variable transport properties. The system of non-stationary nonlinear energy- and mass-conservation equations is solved using the method of lines. The numerical calculations performed are compared with experimental data (Kumagai *et al.* 1971) and recent theoretical models (King 1996; Marchese *et al.* 1999). The Stefan velocity in the neighbourhood of the burning droplet, and the thermophoretic, diffusiophoretic and total velocities of combustion-generated particles are calculated. It is shown that soot particles form the size-segregated soot-shell structure. Within a soot shell the particles with smaller radii are located closer to the droplet surface, while larger particles are located closer to the flame front. Numerical calculations performed for moderately large particles showed that there are two equilibrium locations, where the total velocity of a soot particle is equal to zero, between the droplet and the flame front. It was found that one of the equilibrium locations is the point of unstable equilibrium and the other position is the point of stable equilibrium. We performed numerical calculations of the dependence of soot-shell-to-droplet-diameter ratios (d_s/d) on the radius of a soot particle. Combining the numerical results obtained with the experimental data from Jackson & Avedisian (1994), we found that during droplet combustion the mean soot aggregates' size grows slowly and linearly with time. The analysis performed showed that, since the maximum of Stefan velocity versus normalized coordinate $x = r/R(\tau)$ is constant in time, for the soot particles located in the vicinity of the maximum of Stefan velocity, the soot-shell-to-droplet-diameter ratio d_s/d does not depend on time.

We are indebted to J. B. Greenberg, N. Kleeorin, A. F. Sarofim and F. A. Williams for useful discussions.

Appendix A. Summary of the equations used for calculating physical properties

The density ρ (kg m^{-3}) was calculated using the equation of state of an ideal gas:

$$\rho = \frac{p}{R_\mathrm{g} T \sum_{i=1}^{N} (Y_i/M_i)}. \tag{A 1}$$

The formula for specific heat at constant pressure, $c_{p,i}$ (J kg^{-1} K^{-1}), is given by

$$c_{p,i} = A + B \cdot \tilde{T} + C \cdot \tilde{T}^2 + D \cdot \tilde{T}^3 + \frac{E}{\tilde{T}^2}, \tag{A 2}$$

where $\tilde{T} = T(\mathrm{K})/1000.0$ and A, B, C, D and E denote the constants. The values of these constants for gaseous species and n-heptane can be found in Chase (1998).

In the ideal-gas state, for a gas mixture specific heat at constant pressure (Reid *et al.* 1987) is given by

$$c_p = \sum_{i=1}^{N} y_i c_{p,i}, \tag{A 3}$$

where y_i is the molar fraction of the ith species.

Wilke's correlation is used to determine the diffusion coefficient D_i ($\mathrm{m^2\,s^{-1}}$) (Reid *et al.* 1987) given by

$$D_i = \frac{(1 - y_i)}{\sum_{\substack{j=1 \\ j \neq i}}^{N} (y_j)/\mathcal{D}_{ij}}, \tag{A 4}$$

where y_j is the molar fraction of the jth species and $\mathcal{D}_{ij}$ is the binary diffusion coefficient (in $\mathrm{m^2\,s^{-1}}$) calculated using Fuller's correlation

$$\mathcal{D}_{ij} = \frac{0.143 \times 10^{-6} T^{1.75}}{p^* \sqrt{M_{ij}} [(\sum_v)_i^{1/3} + (\sum_v)_j^{1/3}]^2}, \tag{A 5}$$

where $M_{ij} = 2[(1/M_i) + (1/M_j)]^{-1}$, M_i and M_j are molecular weight ($\mathrm{g\,mol^{-1}}$) of the ith and jth species, respectively, p^* is pressure (bar) and $\sum_v$ is found for each component by summing the atomic diffusion volumes.

The latent heat of evaporation $L(T_\mathrm{S})$ ($\mathrm{J\,kg^{-1}}$) is approximated by (Saitoh *et al.* 1993)

$$L(T_\mathrm{S}) = 5.553 \times 10^4 (T_\mathrm{c} - T_\mathrm{S})^{0.3436}, \tag{A 6}$$

where T_c is the critical temperature of the liquid (Reid *et al.* 1987).

Viscosity, μ_i (10^{-3} Pa s), is approximated by Golubev's equations (Reid *et al.* 1987)

$$\eta_i = \begin{cases} \eta_\mathrm{c}^{(\mathrm{i})} T_{\mathrm{r},i}^{0.965} & \text{for } T_\mathrm{r} < 1, \\ \eta_\mathrm{c}^{(\mathrm{i})} T_{\mathrm{r},i}^{0.71 + 0.29/T_{\mathrm{r},i}} & \text{for } T_\mathrm{r} > 1, \end{cases} \tag{A 7}$$

where $T_\mathrm{r} = T/T_{\mathrm{c},i}$, $\eta_\mathrm{c}^{(\mathrm{i})}$ is the viscosity at critical temperature that can be found from

$$\eta_\mathrm{c}^{(\mathrm{i})} = \frac{3.5 M_i^{1/2} P_{\mathrm{c},i}^{2/3}}{T_{\mathrm{c},i}^{1/6}}, \tag{A 8}$$

where $T_{\mathrm{c},i}$ is the critical temperature and $P_{\mathrm{c},i}$ is the critical pressure.

The viscosity of the gaseous mixture was approximated as (Reid *et al.* 1987)

$$\eta = \sum_{i=1}^{N} \frac{y_i \eta_i}{\sum_{j=1}^{N} y_j \Phi_{ij}}, \tag{A 9}$$

where y_i is the molar fraction of the ith species and Φ_{ij} is found using Wilke's approximation

$$\Phi_{ij} = \frac{[1 + \sqrt{\eta_i/\eta_j}(M_j/M_i)^{1/4}]^2}{2\sqrt{2(1 + M_i/M_j)}}. \tag{A 10}$$

The thermal conductivity of a gaseous mixture, k_{e} ($\mathrm{W\,m^{-1}\,K^{-1}}$), was approximated by Wassiljewa's equation (Reid *et al*. 1987)

$$k_{\mathrm{e}} = \sum_{i=1}^{N} \frac{y_i k_i}{\sum_{j=1}^{N} y_j A_{ij}}, \tag{A 11}$$

where k_i is the thermal conductivity of the ith species, y_i and y_j are the molar fractions of ith and jth species, respectively, and A_{ij} can be calculated from the Lindsay–Bromley correlation (Reid *et al*. 1987)

$$A_{ij} = \frac{1}{4}\left(1 + \sqrt{\frac{\eta_i}{\eta_j}\left(\frac{M_j}{M_i}\right)^{3/4}\frac{T+S_i}{T+S_j}}\right)^2 \frac{T+S_{ij}}{T+S_j}, \tag{A 12}$$

where S_i, S_{ij} and S_{ij} are the Sutherland constants given by $S_i = 1.5T_{\mathrm{b},i}$ and $S_{ij} = \sqrt{S_i S_j}$ and $T_{\mathrm{b},i}$ is the boiling point of the ith species.

Nomenclature

C_2	second Planck constant
c_p	specific heat at a constant pressure
c	sound velocity
d	diameter
D_{f}	fractal dimension
D_i	diffusion coefficient of ith species
$\mathcal{D}_{ij}$	mutual diffusion coefficient
E_{a}	activation energy
E_{b}	black-body-emitted flux
f_{v}	soot volume fraction
f_{T}	thermophoretic coefficient
I	radiation intensity
k	thermal conductivity
K_{b}	burning rate constant
K_{tsl}	coefficient of thermal slip
Kn	Knudsen number
L	latent heat of evaporation
l	path length
M_i	molecular weight of species i
m_i	mass of the ith species molecule
p	pressure
$\boldsymbol{Q}_{\mathrm{R}}$	radiation flux vector
Q	specific heat of chemical reaction
r	radial coordinate
R	radius of the droplet
R_{p}	radius of the particle

R_{g}	universal gas constant
T	temperature
t	time
u, v	velocity
Y	mass fraction
y	molar fraction
Z	pre-exponential constant
Greek symbols	
α^*	momentum accommodation coefficient
α_{ij}	multicomponent thermal diffusion factor
α_{l}	liquid thermal diffusivity
$\boldsymbol{\varepsilon}$	energy accommodation coefficient
ϵ	emissivity
κ_{P}	Planck mean absorption coefficient
λ	mean free path
μ	dynamic viscosity
ν_i'', ν_i'	stoichiometric coefficients of the products and reactants
ρ	density
$\dot{\omega}$	chemical reaction rate
Subscripts and superscripts	
F	fuel
i	number of a species
l	liquid
o	oxidizer
p	particle
S	value at the droplet surface
s	soot
sp	solid phase
∞	value at infinity

References

Abdel-Khalik, S. I., Tamaru, T. & El-Wakil, M. M. 1974 A chromatographic and interferometric study of the diffusion flame around a simulated fuel drop. In *Proc. 15th Int. Symp. on Combustion*, pp. 389–399. Pittsburgh: The Combustion Institute.

Avedisian, C. T. 1997 Soot formation in spherically symmetric droplet combustion. In *Physical and chemical aspects of combustion* (ed. F. L. Dryer & R. F. Sawyer), ch. 6, pp. 135–160. Amsterdam: Gordon & Breach.

Avedisian, C. T. & Callahan, B. J. 2000 Experimental study of nonane–hexanol mixture droplet combustion without natural or forced convection. In *Proc. 28th Int. Symp. on Combustion*, pp. 991–997. Pittsburgh: The Combustion Institute.

Avedisian, C. T., Callahan, B. J. & Jackson, G. S. 1998 Soot shell structures of fuel droplet flames in microgravity. *Trans. ASME J. Heat Transfer* **120**, 544.

Baek, S. W., Park, J. H. & Choi, C. H. 1999 Investigation of droplet combustion with nongray gas radiation effects. *Combust. Sci. Technol.* **142**, 55–79.

Bakanov, S. P. 1992 Thermophoresis in gases at small Knudsen numbers. *Phys. Usp. Usp. Fiz. Nauk.* **35**, 783–792.

Bakanov, S. P. 1995 Future directions for experiments in thermophoresis: a commentary. *J. Aerosol Sci.* **26**, 1–4.

Bakanov, S. P., Derjaguin, B. V. & Roldughin, V. I. 1979 Thermophoresis in gases. *Phys. Usp. Usp. Fiz. Nauk.* **22**, 813–825.

Ben-Dor, G., Elperin, T. & Krasovitov, B. 2003 Numerical analysis of the effects of temperature and concentration jumps on transient evaporation of moderately large ($0.01 \lesssim Kn \lesssim 0.3$) droplets in non-isothermal multicomponent gaseous mixtures. *Heat Mass Transfer*. (In the press.)

Brasil, A. M., Farias, T. L., Carvalho, M. G. & Koylu, U. O. 2001 Numerical characterization of the morphology of aggregated particles. *J. Aerosol Sci.* **32**, 489–508.

Brock, J. R. 1962 On the theory of thermal forces acting on aerosol particles. *J. Colloid Sci.* **17**, 768–770.

Chang, K. C. & Shien, J. S. 1995 Theoretical investigation of transient droplet combustion by consuidering flame radiation. *Int. J. Heat Mass Transfer* **38**, 2611–2621.

Chase Jr, M. W. 1998 NIST–JANAF thermochemical tables. 4th edn. *J. Phys. Chem. Ref. Data* **9**, 1–1951.

Choi, M. Y., Mulholland, G. W., Hamins, A. & Kashiwagi, T. 1995 Comparison of the soot fraction using gravimetric and light extinction techniques. *Combust. Flame* **102**, 161–169.

Ezekoye, O. A. & Zhang, Z. 1997 Soot oxidation and agglomeration modeling in a microgravity diffusion flame. *Combust. Flame* **110**, 127–139.

Felske, J. D. & Tien, C. L. 1973 Calculations of the emissivity of luminous flames. *Combust. Sci. Technol.* **7**, 25–31.

Hara, H. & Kumagai, S. 1990 Experimental investigation of free droplet combustion under microgravity. In *Proc. 23rd Int. Symp. on Combustion*, pp. 1065–1611. Pittsburgh: The Combustion Institute.

Hubbard, G. L., Denny, V. E. & Mills, A. F. 1975 Droplet evaporation: effect of transients and variable properties. *Int. J. Heat Mass Transfer* **18**, 1003–1008.

Jackson, G. S. & Avedisian, C. T. 1994 The effect of initial diameter in spherically symmetric droplet combustion of sooting fuels. *Proc. R. Soc. Lond.* A **446**, 255–276.

Jackson, G. S. & Avedisian, C. T. 1996 Modeling of spherically symmetric droplet flames including complex chemistry: effect of water addition on *n*-heptane combustion. *Combust. Sci. Technol.* **115**, 125–149.

Jackson, G. S., Avedisian, C. T. & Yang, J. C. 1991 Soot formation during combustion of unsupported methanol/toluene mixture droplets in microgravity. *Proc. R. Soc. Lond.* A **435**, 359–369.

Jackson, G. S., Avedisian, C. T. & Yang, J. C. 1992 Observation of soot during droplet combustion at low gravity: heptane/monochloroalkane mixtures. *Int. J. Heat Mass Transfer* **35**, 2017–2033.

Kadota, T. & Hiroyasu, H. 1984 Soot concentration measurement in a fuel droplet flame via laser light scattering. *Combust. Flame* **55**, 195–201.

Kadota, T., Hiroyasu, H. & Farazandehemhr, A. 1977 Soot formation by combustion of a fuel droplet in high pressure gaseous environments. *Combust. Flame* **29**, 67–75.

King, M. K. 1996 An unsteady-state analysis of porous sphere and droplet fuel combustion under microgravity conditions. In *Proc. 26th Int. Symp. on Combustion*, pp. 1227–1234. Pittsburgh: The Combustion Institute.

Köylü, Ü. Ö., Xing, Y. & Rosner, D. E. 1995*a* Fractal morphology analysis of combustion-generated aggregates using angular light scattering and electron microscope images. *Langmuir* **11**, 4848–4854.

Köylü, Ü. Ö., Faeth, G. M., Farias, T. L. & Carvalho, M. G. 1995*b* Fractal and projected properties of soot aggregates. *Combust. Flame* **100**, 621–633.

Krupitczka, R. 1967 Analysis of thermal conductivity in granular materials. *Int. Chem. Engng* **7**, 122–144.

Kumagai, S., Sakai, T. & Okajima, S. 1971 Combustion of free fuel droplets in a freely falling chamber. In *Proc. 13th Int. Symp. on Combustion*, pp. 779–785. Pittsburgh: The Combustion Institute.

Law, C. K. 1982 Recent advances in droplet vaporization and combustion. *Prog. Energy Combust. Sci.* **8**, 171–201.

Lee, K. Y., Zhong, Z. Y. & Tien, C. L. 1984 Blockage of thermal radiation by the soot layer in combustion of condensed fuels. *Proc. 12th Symp. Int. on Combustion*, pp. 1629–1636. Pittsburgh: The Combustion Institute.

Loyalka, S. K. 1992, Thermophoretic force on a single particle. I. Numerical solution of the linerized Boltzmann equation. *J. Aerosol Sci.* **23**, 291–300.

Manzello, S. L. & Choi, M. Y. 2002 Morphology of soot collected in microgravity droplet flames, *Int. J. Heat Mass Transfer* **45**, 1109–1116.

Marchese, A. J. & Dryer, F. L. 1996 The effect of liquid mass transport on the combustion and extinction of bicomponent droplets of methanol and water. *Combust. Flame* **105**, 104–122.

Marchese, A. J., Dryer, F. L. & Nayagam, V. 1999 Numerical modeling of isolated *n*-alkane droplet flames: initial comparison with ground and space-based microgravity experiments. *Combust. Flame* **116**, 432–459.

Nayagam, V., Haggard Jr, J. B., Colantonio, R. O., Marchese, A. J., Dryer, F. L., Zhang, B. L. & Williams, F. A. 1999 Microgravity *n*-heptane droplet combustion in oxygen–helium mixtures at atmospheric pressure. *AIAA J.* **36**, 1369–1378.

Poddoskin, A. B., Yushkanov, A. A. & Yalamov, Yu. I. 1982 Theory of thermophoresis of moderately large aerosol particles. *Sov. Phys. Tech. Phys.* **27**, 1383–1388.

Randolph, A. L. & Law, C. K. 1986 Influence of physical mechanisms on soot formation and destruction in droplet burning. *Combust. Flame* **64**, 267–284.

Reid, R. C., Prausnitz, J. M. & Poling, B. E. 1987 *The properties of gases and liquids*, 4th edn. New York: McGraw-Hill.

Roekaerts, D., Teerling, J. & Merci, B. 2000 Note in preparation of a discussion on the role of turbulence model and inlet profiles in computations of piloted jet flame D. In *Proc. 5th Int. Workshop on Measurement and Computation of Turbulent Nonpremixed Flames* (ed. A. Mbiock, D. Roekaerts & R. Barlow), pp. 121–124. Delft: Delft University of Technology.

Ronney, P. D. 1998 Understanding combustion processes through microgravity research (invited plenary lecture). In *Proc. 27th Int. Symp. on Combustion*, pp. 2485–2506. Pittsburgh: The Combustion Institute.

Saitoh, T., Yamazaki, K. & Viskanta, R. J. 1993 Effect of thermal radiation on transient combustion of a fuel droplet. *J. Thermophys. Heat Transfer* **7**, 94–100.

Shaw, B. D., Dryer, F. L., Williams, F. A. & Haggard Jr, J. B. 1988 Sooting and disruption in spherically symmetrical combustion of decane droplets in air. *Acta Astronautica* **17**, 1195–1202.

Siegel, R. & Howell, J. R. 1981 *Thermal radiation heat transfer*, 2nd edn, ch. 17. New York: Hemisphere.

Sincovec, R. F. & Madsen, N. K. 1975 Software for nonlinear partial differential equations. *ACM Trans. Math. Software* **1**, 232–260.

Talbot, L., Cheng, R. K., Schefer, R. W. & Willis, D. R. 1980 Thermophoresis of particles in heated boundary layer. *J. Fluid Mech.* **101**, 737–758.

Vargaftik, N. B. 1975 *Tables on the thermophysical properties of liquids and gases*, 2nd edn. New York: Halsted Press.

Viehland, L. A. & Mason, E. A. 1977 Phoresis of spherical particles in multicomponent gas mixtures. *J. Aerosol Sci.* **8**, 381–385.

Waldman, L. 1959 Über die Kraft eines inhomogenen Gases auf kleine suspendierte Kugeln. *Zeitschrift Naturforschung* **14a**, 589–599.

Westbrook, C. K. & Dryer, F. L. 1981 Simplified reaction mechanism for the oxidation of hydrocarbon fuels. *Combust. Sci. Technol.* **27**, 31–43.

Williams, F. A., Dietrich, D. L., Haggard Jr, J. B., Dryer, F. L., Nayagam, V. & Shaw, B. D. 1996 Fiber supported droplet combustion (FSDC). In The Second United States Microgravity Laboratory 90-day Science Report, March 1996, pp. 87–88. Huntsville, AL: Marshall Space Flight Center.

Yalamov, Y. I., Vasiljeva, L. Y. & Schukin, E. R. 1977 The study of various mechanisms of incloud scavenging of large, moderately large, and small aerosol particles. *J. Colloid Interface Sci.* **62**, 503–508.

Yamamoto, K. & Ishihara, Y. 1988 Thermophoresis of spherical particle in a rarefied gas of a transition regime. *Phys. Fluids* **31**, 3618–3624.

Zheng, F. & Davis, E. J. 2001 Thermophoretic force measurements of aggregates of microspheres. *J. Aerosol Sci.* **32**, 1421–1435.